

Flatsonium: Charge and flux insensitive tunable superconducting qubit

Eyob A. Sete,* Matthew J. Reagor, Nicolas Didier, and Chad T. Rigetti
Rigetti & Co., Inc.
775 Heinz Avenue, Berkeley, CA 94710
(Dated: April 20, 2022)

Superconducting qubits with in-situ tunable properties are important capabilities for constructing quantum computer. But, tunability often comes at the expense of increased noise sensitivity for the qubits. Here, we propose a flux-tunable superconducting qubit that minimizes the dephasing due to the global flux-noise by engineering controllable “flux sweet spots” at frequencies of interest. This is realized by using SQUID with asymmetric junctions shunted by an superconductor formed from array of Josephson junctions. When the main contribution to the magnetic flux noise comes from the global fluctuations of the magnetic field, it is possible to achieve several orders of magnitude improvement in dephasing time. The proposed qubit can be used to realize fast, high-fidelity two-qubit gates in large scale quantum processors, a key ingredient for implementing fault-tolerant quantum computers.

I. INTRODUCTION

Superconducting qubits are promising components for the construction of practical quantum computers. A persistent challenge is two-qubit gate errors, in particular for multi-qubit entangling operations. It is desirable to have long coherence times and fast, accurate controls. However, achieving both objectives at once has been difficult for superconducting qubits. Some architectures rely on fixed-frequency qubits with static qubit-qubit coupling. While such systems exhibit long coherence times approaching $100 \mu\text{s}$, two-qubit gates are typically hundred-nanoseconds in duration, limiting fidelities so far to $F = 99.1\%$ [1–3]. Other architectures rely on frequency tunable qubits, which often have shorter coherence times $20 - 50 \mu\text{s}$, but faster two-qubit gates, tens of nanoseconds in duration, limiting fidelities thus far to $F = 99.44\%$ [4, 5]. Fluctuations of qubit frequency due to flux noise significantly affect coherence times [6–8]. Additionally, most flux-tunable based two-qubit gates are implemented using slightly anharmonic qubits, which places limits on control accuracy or leakage to upper levels [9]. Achieving flux-insensitivity with tunable, highly anharmonic qubits could further bolster superconducting qubit technologies.

In this work, we propose a superconducting qubit design based on a fluxonium [10–13] with engineered *flux sweet spots*. Its strong nonlinearity, tunability and insensitivity to noise at the frequency of operations makes the qubit a candidate for realizing fast, high fidelity two-qubit operations. The circuit model of the qubit device consists of a superconducting quantum interference device (SQUID) shunted using an array of Josephson junctions, thus forming two loops—A and B. (see Fig. 1). The qubit’s energy spectrum is controlled by the magnetic flux threading through loops A and B. In addition to the sweet spots at the minimum and maximum frequencies, already present in the fluxonium, a number of sweet spots can be realized when the SQUID has asymmetric junction energies and the magnetic fluxes through loops A and B are related as integer multiples. The number and positions of

the sweet spots can be controlled by tuning the Josephson energy asymmetry and the area of the loops. The qubit has a wide tunable frequency range $\sim 0.5\text{--}10$ GHz for realistic parameter regime. Our numerical simulations show that when operated at the flux sweet spots, the qubit exhibits several orders of magnitude improvement in dephasing time, T_ϕ than that of the corresponding fluxonium, assuming that flux-noise is global in nature.

II. MODEL AND HAMILTONIAN

A fluxonium qubit provides broad frequency tunability and large anharmonicity, allowing construction of fast, high fidelity two-qubit gates. All flux tunable qubits are susceptible to flux noise. It has recently been shown that by increasing the asymmetry of the junction energies in a transmon qubit, it is possible to create flux-insensitive points [14, 15], yielding coherence time that is nearly flux independent [15]. In the case of fluxonium, although the T_1 time can reach to a few milliseconds when biased at the half-flux quantum [16], the dephasing time T_2 at frequency of interest is mostly limited by flux noise [11, 16]. Here, we propose a qubit design that comprises a SQUID loop shunted by an array of Josephson junctions (see Fig. 1) and has a flat $|0\rangle \rightarrow |1\rangle$ transition spectrum at the frequency of operation. Hence the choice of the name for our qubit—“flatsonium.”

The proposed circuit consists of a superconducting loop formed by two Josephson junctions of Josephson energies E_{J1} and E_{J2} with its total intrinsic capacitance C_J . The superconducting loop A is shunted by an array of Josephson junctions acting as a superinductor of inductance L_A . The external flux threading through loop A is Φ_1 and the flux through loop B is Φ_2 . Following the method outlined in Ref. [17], the circuit Hamiltonian for flatsonium can be written as

$$H = 4E_C n^2 - E_{J1} \cos \phi - E_{J2} \cos(\phi + 2\pi\Phi_1/\Phi_0) + \frac{1}{2}E_L(\phi + 2\pi\Phi_1/\Phi_0 + 2\pi\Phi_2/\Phi_0)^2, \quad (1)$$

where n is the number of Cooper pairs that have tunneled through the junctions, $\phi = 2\pi\Phi/\Phi_0$ is the phase difference between the two nodes (2π -periodic) with $\Phi_0 = h/2e$ the flux

* eyob@rigetti.com

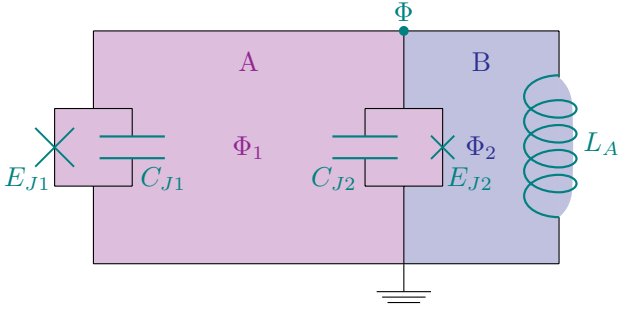


Figure 1. Flatsonium qubit circuit diagram. The circuit consists of a SQUID loop formed by two Josephson junctions of Josephson energies E_{J1} , E_{J2} and total capacitance $C_J = C_{J1} + C_{J2}$. An external magnetic field produces the magnetic flux Φ_1 through the SQUID (loop A). The SQUID is in turn shunted by an array of Josephson junctions represented by a linear inductor of inductance L_A . The area of the loop enclosed by the array inductance L_A and the right SQUID arm is biased by the magnetic flux Φ_2 (loop B). Three branches yield distinct paths from the node Φ to the ground node, through the Josephson junctions and the superinductor, and lead to the Hamiltonian Eq. (1).

quantum. Similarly we note $\phi_{j=1,2} = 2\pi\Phi_j/\Phi_0$. The Hamiltonian is characterized by the Josephson energies, the charging energy $E_C = e^2/2C_J$ of the Josephson junctions and the inductance energy $E_L = (\Phi_0/2\pi)^2/L_A$ of the Josephson junctions array.

We may redefine ϕ to move the external flux dependence to the Josephson terms altogether: $\varphi = \phi + \phi_1 + \phi_2$ and obtain

$$H = 4E_C n^2 - E_{J1} \cos(\varphi - \phi_1 - \phi_2) - E_{J2} \cos(\varphi - \phi_2) + \frac{1}{2} E_L \varphi^2. \quad (2)$$

In the quantum regime, the number \hat{n} of Cooper pairs and the phase $\hat{\varphi}$ are canonical conjugate variables that satisfy the commutation relation $[\hat{n}, \hat{\varphi}] = i$.

Let us assume that the external fluxes through the loops have a general relation $\Phi_1 = r\Phi_2$, $r \in \mathbb{R}$. In view of this and applying a trigonometric relation, the Hamiltonian can be written in the form

$$H = 4E_C \hat{n}^2 - E_{J,\text{eff}}(\phi_2) \cos(\hat{\varphi} - \varphi_0) + \frac{E_L}{2} \hat{\varphi}^2, \quad (3)$$

where the Josephson potential is controlled by the external magnetic fields as follows,

$$E_{J,\text{eff}}(\phi_2) = \frac{E_{J\Sigma}}{1+b} \sqrt{1+b^2+2b\cos(r\phi_2)}, \quad (4)$$

$$\varphi_0 = \arctan \left[\frac{b \sin \phi_2 + \sin[(1+r)\phi_2]}{b \cos \phi_2 + \cos[(1+r)\phi_2]} \right]. \quad (5)$$

We define the Josephson junction energy asymmetry parameter $b = E_{J2}/E_{J1}$ and $E_{J\Sigma} = E_{J1} + E_{J2} = E_{J1}(1+b)$ the total Josephson junction energy. The relation between the two fluxes $\Phi_1 = r\Phi_2$ can be achieved in two ways: global flux biasing and on-chip flux biasing. In the case of global

flux biasing, a constant magnetic field is applied by placing a large coil beneath or around the qubit chip. The parameter r can then be controlled by changing the areas of the loops. In the case of on-chip flux biasing, a magnetic field is applied locally through current carrying wire on-chip. Since the magnetic fluxes through the two loops are variable, the parameter r is controlled by the applied magnetic field and the area of the loops.

The fluxonium Hamiltonian can be recovered from Eq. (3) by setting $b = 0$ and $r = 0$:

$$H_F = 4E_C \hat{n}^2 - E_{J\Sigma} \cos(\hat{\varphi} - \phi_2) + \frac{E_L}{2} \hat{\varphi}^2, \quad (6)$$

with the effective junction energy $E_{J\Sigma}$. This Hamiltonian has been shown to have strong anharmonic energy spectrum [10]. The $|0\rangle \rightarrow |1\rangle$ transition frequency f_{01} has a wide tunability as a function of external fluxes and has flux sweet spots at $\phi_2 = m\pi$, where $m \in \mathbb{Z}$. The frequency has a linear dependence on the applied magnetic flux away from the sweet spots (blue curve in Fig. 2) and is approximately given by $f_{01} \approx 4\pi^2 E_L E_{J\Sigma} |1/2 - \phi_2/2\pi| / h(E_L + E_{J\Sigma})$ [10]. Note that the fluxonium qubit energy parameters broadly fall in the range: $E_L \ll E_C \ll E_{J\Sigma}$ with $2 \lesssim E_{J\Sigma}/E_C \lesssim 5$ [10, 12, 13]. While the energy relaxation time T_1 of a fluxonium qubit at operating frequency (4–8 GHz) is comparable or better than that of transmon qubits [11, 18], the dephasing time is still very sensitive to flux noise and is limited to a few microseconds [11]. In the following, we discuss how to improve T_2 time by introducing *engineered flux sweet spots* at the frequency of operation.

In addition to the flux sweet spots at zero-flux, half-flux, and one-flux quantum values, other flux sweet spots can be created by introducing asymmetry in the SQUID junction energies and the external magnetic fluxes. It turns out that for the circuit shown in Fig. 1, periodic flux sweet spots and a symmetric energy spectrum can be obtained when the asymmetry parameter of the two junction energies satisfies $b = r + 1$, where r and b are integer values. Note that flux sweet spots can also be created for non-integer r values. However, the resulting spectrum is not symmetric about the half flux-quantum bias point.

In the f_{01} transition frequency, the flux sweet spots appear at the minima of the effective potential $U(\hat{\varphi}) = E_L \hat{\varphi}^2/2 - E_{J,\text{eff}} \cos(\hat{\varphi} - \varphi_0)$. Setting the first derivative of the potential to zero, $\partial U(\varphi_0)/\partial \phi_2 = 0$, we find the condition for the flux sweet spots to be $\phi_2/2\pi = m/2r$, where $m \in \mathbb{Z}$. The total number of flux sweet spots n_{sp} within one flux-quantum is given by (for $r > 1$)

$$n_{\text{sp}} = \begin{cases} r + 4, & \text{for odd } r, \\ r + 3, & \text{for even } r, \end{cases} \quad (7)$$

where we have included the flux sweet spots at zero and at one flux quantum ($m = 0, 1, \dots, 2r$).

In order to discuss of notion of flux sweet spots, it is more convenient to introduce common mode $\Phi_{\text{sum}} = \Phi_1 + \Phi_2$ and differential mode $\Phi_{\text{diff}} = \Phi_1 - \Phi_2$. In view of the relation $\Phi_1 = r\Phi_2$, the common and differential mode variables are related as $\Phi_{\text{diff}} = \beta\Phi_{\text{sum}}$, where $\beta = (r-1)/(r+1)$.

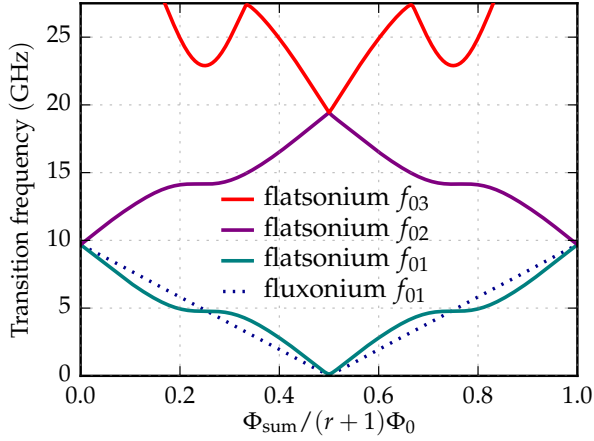


Figure 2. The first three transition frequencies of the flatsonium qubit for $E_C/h = 6$ GHz, $E_L/h = 0.5$ GHz, $E_{J\Sigma}/h = (b+1)E_{J1}/h = 20$ GHz, for flux asymmetry $r = 2$ (which corresponds to junction energy asymmetry $b = r + 1 = 3$).

The energy spectrum of the flatsonium qubit can be obtained by numerically diagonalizing the Hamiltonian Eq. (3). Because of the bosonic commutation rule between \hat{n} and $\hat{\varphi}$, it is more convenient to use the Fock basis by writing these conjugate operators as the two quadratures of a harmonic oscillator that is rendered nonlinear by the Josephson junctions. Using the first 50 Fock states and energy parameters $E_L/h = 0.5$ GHz, $E_C/h = 6$ GHz, $E_{J\Sigma}/h = 20$ GHz, and for loop area asymmetry $r = 2$ ($\beta = 1/3$) and junction symmetry $b = r + 1 = 3$, the results of the numerical diagonalization is shown in Fig. 2. The blue line represents the fluxonium f_{01} frequency, which corresponds to a SQUID with symmetric junctions, obtained by setting $r = 0$ and $b = 0$. The rest of the curves represent the first three transition frequencies of flatsonium. The f_{01} transition frequency (cyan curve) has two additional flux sweet spots within one-flux quantum, as expected from Eq. (7). The position of these flux sweet spots are $\Phi_{\text{sum}}/(r+1)\Phi_0 = 1/4, 3/4$, which are on either side of the minimum frequency point. Note also that the anharmonic energy spectrum feature is still intact, making the device a good approximation of a two-level system.

III. DEPHASING DUE TO FLUX NOISE

In general, dephasing is understood as the fluctuation of the qubit frequency due to coupling to the environment. Low frequency noise far below the transition frequency can cause the qubit to accumulate a random phase. It is well known that flux tunable qubits such as flux and fluxonium qubits are susceptible to flux noise. This is due to the fact that fluctuations in flux induce fluctuations in the qubit frequency, resulting in dephasing. This leads to short dephasing T_2 time. The sensitivity of the qubit frequency to flux noise can be suppressed by engineering flux sweet spots. For external flux bias these fluctuations can be induced by a global flux noise (caused by a fluctuating magnetic field) and/or a local flux noise, for exam-

ple, caused by fluctuating spins at the surface of the superconductor [19] or in defects at the metal-insulator interface [20].

In the case of weak fluctuations, each external parameter in the qubit Hamiltonian can be decomposed into its controlled DC value and fluctuations around it. For the external flux, we can write $\Phi_{\text{sum}} = \Phi_{\text{sum}}^{(0)} + \delta\Phi_{\text{sum}}$ and $\Phi_{\text{diff}} = \Phi_{\text{diff}}^{(0)} - \delta\Phi_{\text{diff}}$. The Hamiltonian of the qubit, expressed in terms of Pauli operators, can be expanded in a Taylor series as

$$H = \frac{\hbar}{2} \left[\omega_{01} + \frac{\partial\omega_{01}}{\partial\Phi_{\text{sum}}} \delta\Phi_{\text{sum}} + \frac{\partial\omega_{01}}{\partial\Phi_{\text{diff}}} \delta\Phi_{\text{diff}} + \dots \right] \hat{\sigma}_z. \quad (8)$$

The fluctuation generally results in two distinct effects: For sufficiently low frequencies, the fluctuations cause random shifts of the transition frequency of the qubit, leading to pure dephasing (time scale T_2); for higher frequencies, the fluctuations induce transition between the qubit states, leading to energy relaxation (time scale T_1). In the following we focus on reducing the pure dephasing rate to improve T_2 .

To better understand how the frequency fluctuations degrade T_2 , we calculate the decay rate of the off-diagonal density matrix element, which is given by $\rho_{01}(t) = e^{i\omega_{01}t} \langle e^{i\delta v(t)} \rangle$,

$$\delta v(t) = \frac{\partial\omega_{01}}{\partial\Phi_{\text{sum}}} \int_0^t dt' \delta\Phi_{\text{sum}}(t') + \frac{\partial\omega_{01}}{\partial\Phi_{\text{diff}}} \int_0^t dt' \delta\Phi_{\text{diff}}(t'), \quad (9)$$

where $\delta v(t)$ is the random phase accumulated. Assuming Gaussian noise, $\langle e^{i\delta v(t)} \rangle = e^{-\frac{1}{2}\langle \delta v^2 \rangle}$, the decay rate is then obtained using

$$\begin{aligned} \langle \delta v^2 \rangle &= \left(\frac{\partial\omega_{01}}{\partial\Phi_{\text{sum}}} t \right)^2 \int_{-\infty}^{\infty} d\omega \text{sinc}^2(\frac{1}{2}\omega t) S_{\Phi_{\text{sum}}}(\omega) \\ &+ \left(\frac{\partial\omega_{01}}{\partial\Phi_{\text{diff}}} t \right)^2 \int_{-\infty}^{\infty} d\omega \text{sinc}^2(\frac{1}{2}\omega t) S_{\Phi_{\text{diff}}}(\omega) \end{aligned} \quad (10)$$

In flux tunable devices, flux noise is mostly dominated by $1/f$ noise whose spectral density is given by [19]

$$S_{\Phi}(f) = A_{\Phi}^2 / f^{\alpha}, \quad (11)$$

where $0.8 \lesssim \alpha \lesssim 1.3$. The parameter A_{Φ} determines the overall amplitude of the fluctuations and has been measured in various experiments [4, 21–26] with values ranging in $A_{\Phi} = 10^{-6}\Phi_0 - 10^{-5}\Phi_0$. Introducing infrared and ultraviolet cut-off frequencies ω_{ir} and ω_{uv} , the dephasing becomes

$$\langle \delta v^2 \rangle = 2 \left[\left(A_{\Phi_{\text{sum}}} \frac{\partial\omega_{01}}{\partial\Phi_{\text{sum}}} t \right)^2 + \left(A_{\Phi_{\text{diff}}} \frac{\partial\omega_{01}}{\partial\Phi_{\text{diff}}} t \right)^2 \right] |\ln \omega_{\text{ir}} t|, \quad (12)$$

which is valid for $\omega_{\text{ir}} t \ll 1$ and $\omega_{\text{uv}} t \gg 1$. The first order dephasing due to flux noise is then given by

$$\Gamma_{\phi} \simeq \Gamma_{\phi, \text{sum}} + \Gamma_{\phi, \text{diff}}, \quad (13)$$

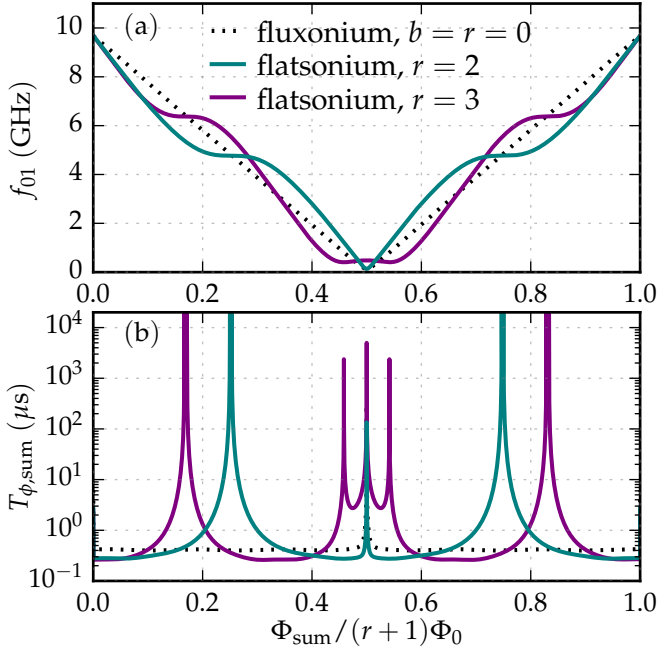


Figure 3. (a) The $|0\rangle \rightarrow |1\rangle$ transition frequency of the fluxonium qubit (blue) and the flatsonium qubit ($r = 2$ in cyan, $r = 3$ in magenta) as a function of the total external flux the loops. Parameters are $E_{J\Sigma}/h = 20$ GHz, $E_L/h = 0.5$ GHz, and $E_C/h = 6$ GHz. (b) Dephasing time $T_{\phi,\text{sum}} = 1/\Gamma_{\phi,\text{sum}}$ [Eq. (14)] for the fluxonium and flatsonium qubits. Here, we have used $A_{\Phi_{\text{sum}}} = 5 \mu\Phi_0$ for the common-mode noise and no differential-mode noise, $A_{\Phi_{\text{diff}}} = 0$.

where

$$\Gamma_{\phi,\text{sum}} = 2\pi A_{\Phi_{\text{sum}}} \sqrt{|\ln(\omega_{ir}t)|} \left| \frac{\partial f_{01}}{\partial \Phi_{\text{sum}}} \right|, \quad (14)$$

$$\Gamma_{\phi,\text{diff}} = 2\pi A_{\Phi_{\text{diff}}} \sqrt{|\ln(\omega_{ir}t)|} \left| \frac{\partial f_{01}}{\partial \Phi_{\text{diff}}} \right|, \quad (15)$$

where $\sqrt{|\ln(\omega_{ir}t)|} \sim 4$ [8, 15]. For general relation between the two fluxes defined earlier, $\Phi_{\text{diff}} = \beta\Phi_{\text{sum}}$, we can re-write the dephasing rate due to the local noise as

$$\Gamma_{\phi,\text{diff}} = 2\pi A_{\Phi_{\text{diff}}} \frac{\sqrt{|\ln(\omega_{ir}t)|}}{\Phi_{\text{sum}}} \left| \frac{\partial f_{01}}{\partial \beta} \right|. \quad (16)$$

It has recently been shown that the global noise exclusively induces common-mode noise while the local noise can induce both common-mode and differential-mode noise [8].

The total dephasing rate due to flux noise is related to T_2 as

$$\frac{1}{T_2} = \frac{1}{2T_1} + \Gamma_{\phi} + \Gamma_{\text{other}}. \quad (17)$$

At the flux sweet spots, T_2 approaches the limit set by the energy relaxation T_1 and other dephasing rates, Γ_{other} due to, for example, charge noise, critical current noise, etc [8].

The dephasing time $T_{\phi,\text{sum}} = 1/\Gamma_{\phi,\text{sum}}$ induced by qubit-frequency fluctuations due to global flux noise for the flatsonium and the fluxonium qubits are shown in Fig. 3 for realistic

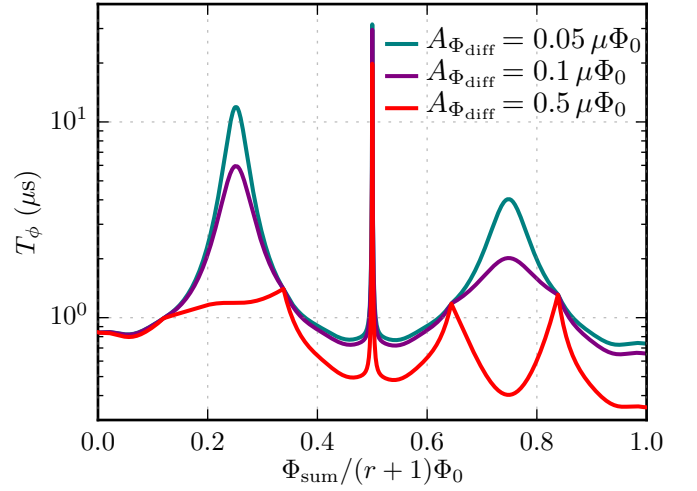


Figure 4. Total dephasing ($1/T_{\phi} = 1/\Gamma_{\phi}$) time versus total flux threading through the two loops with $r = 2$. We have used the global noise amplitude $A_{\Phi_{\text{sum}}} = 5 \mu\Phi_0$ and for different values of the local noise amplitude $A_{\Phi_{\text{diff}}}$. All other parameters are the same as in Fig. 3.

parameters [11]. For the fluxonium, due to the linear dependence on the externally applied flux, the dephasing time is constant and limited to $\sim 1 \mu\text{s}$ away from the sweet spot at $\Phi_{\text{sum}}/\Phi_0 = 1/2$). If we let the SQUID junctions to be asymmetric such that $b = 3$ and the asymmetry of fluxes $r = 2$, we get two additional flux sweet spots for the flatsonium (at $\Phi_{\text{sum}}/(r+1)\Phi_0 = 1/4, 3/4$) as illustrated in Fig. 3 (a) (cyan curve). The corresponding dephasing time [3 (b)] at these flux sweet spots is $1/T_{\phi} \sim 10\text{ms}$, an improvement by nearly four orders of magnitude. Increasing the junction asymmetry to $b = 4$ ($r = 3$), two more flux sweet spots close to the half-flux quantum point are created (magenta curve). This is consistent with our prediction in Eq. (7). Note that the position of the other two flux sweet spots move away from the half-flux quantum point and appear at a higher frequency. The dephasing time is still more than 1 ms.

It has been shown for a device with similar circuit topology that the differential mode can be sensitive to local noise and global noise [8]. In Fig. 4, we show the contribution of both global noise and local noise to the dephasing time for different values of the local noise amplitude $A_{\Phi_{\text{diff}}}$. Although the qubit is insensitive to the global noise at integer multiples of half-flux quantum, the dephasing at the engineered flux sweet spots is limited by the local noise. Suitable surface passivation and improvements in the sample vacuum environment have lead to significant reductions in the surface spin susceptibility and low-frequency flux noise power [27]. Mitigating the local noise is essential in realizing improved coherence time at the engineered flux sweet spots.

IV. CONCLUSION

We have analyzed a new tunable superconducting qubit design with engineered flux sweet spots, which we call flatonium. The qubit circuit consists of a SQUID with asymmetric Josephson junctions shunted by an array of Josephson junctions. The qubit is tuned by an external magnetic flux threading through the SQUID and the Josephson junction array loops. With the appropriate choice of Josephson junctions and loop parameters, the low energy spectrum of the flatonium exhibits a wide tunability and flux sweet spots in

the range of the frequencies of interest. The SQUID Josephson junction asymmetry and the ratio of the magnetic fluxes threading the loops determine the number and position of the flux sweet spots within one flux quantum. Assuming that the main contribution to the low frequency noise comes from the global noise, the dephasing time (at the sweet spots) can improve by several order of magnitude from that of the corresponding fluxonium qubit at the same flux bias point. Its tunability, strong anharmonicity, charge noise insensitivity [10] (due to the large inductance) together with the engineered flux sweet spots make the flatonium qubit a highly coherent device and a potential candidate for constructing fast, high fidelity quantum logic gates.

-
- [1] Jerry M. Chow, Jay M. Gambetta, Easwar Magesan, David W. Abraham, Andrew W. Cross, B. R. Johnson, Nicholas A. Masluk, Colm A. Ryan, John A. Smolin, Srikanth J. Srinivasan, and M. Steffen, *Nature Commun.* **5**, 4015(2014).
- [2] A.D. Córcoles, Easwar Magesan, Srikanth J. Srinivasan, Andrew W. Cross, M. Steffen, Jay M. Gambetta, and Jerry M. Chow, *Nature Commun.* **6**, 6979(2015).
- [3] Maika Takita, A. D. Córcoles, Easwar Magesan, Baleegh Abdo, Markus Brink, Andrew Cross, Jerry M. Chow, and Jay M. Gambetta, *Phys. Rev. Lett.* **117**, 210505(2016).
- [4] R. Barends, J. Kelly, A. Megrant, D. Sank, E. Jeffrey, Y. Chen, Y. Yin, B. Chiaro, J. Mutus, C. Neill, P. O'Malley, P. Roushan, J. Wenner, T. C. White, A. N. Cleland, and John M. Martinis, *Phys. Rev. Lett.* **111**, 080502(2013).
- [5] J. Kelly, A. G. AU Barends, R. Fowler, A. Megrant, E. Jeffrey, T. C. White, D. Sank, J. Y. Mutus, B. Campbell, Yu Chen, Z. Chen, B. Chiaro, A. Dunsworth, I.-C. Hoi, C. Neill, P. J. J. O'Malley, C. Quintana, P. Roushan, A. Vainsencher, J. Wenner, A. N. Cleland, and John M. Martinis, *Nature* **519**, 66 (2015).
- [6] J.M. Martinis and A. Megrant. *arXiv:1410.5793v1*.
- [7] C. M. Quintana, Yu Chen, D. Sank, A. G. Petukhov, T. C. White, Dvir Kafri, B. Chiaro, A. Megrant, R. Barends, B. Campbell, Z. Chen, A. Dunsworth, A. G. Fowler, R. Graff, E. Jeffrey, J. Kelly, E. Lucero, J. Y. Mutus, M. Neeley, C. Neill, P. J. J. O'Malley, P. Roushan, A. Shabani, V. N. Smelyanskiy, A. Vainsencher, J. Wenner, H. Neven, and John M. Martinis, *Phys. Rev. Lett.* **118**, 057702 (2017).
- [8] A. Kou, W.C. Smith, Vool. U., R.T. Brierley, H. Meier, L. Frunzio, S.M. Girvin, L.I. Glazman, and M.H. Devoret. *arXiv:1610.01094v2*.
- [9] Zijun Chen, Julian Kelly, Chris Quintana, R. Barends, B. Campbell, Yu Chen, B. Chiaro, A. Dunsworth, A. G. Fowler, E. Lucero, E. Jeffrey, A. Megrant, J. Mutus, M. Neeley, C. Neill, P. J. J. O'Malley, P. Roushan, D. Sank, A. Vainsencher, J. Wenner, T. C. White, A. N. Korotkov, and John M. Martinis, *Phys. Rev. Lett.* **116**, 020501 (2016).
- [10] Valdimir Manucharyan. *Superinductance*. PhD thesis, Yale University, 2012.
- [11] Vladimir E. Manucharyan, Nicholas A. Masluk, Archana Kamal, Jens Koch, Leonid I. Glazman, and Michel H. Devoret, *Phys. Rev. B* **85**, 024521 (2012).
- [12] Nicholas A. Masluk. *Reducing the losses of the fluxonium artificial atom*. PhD thesis, Yale University, 2012.
- [13] Kurtis Lee Geerlings. *Improving Coherence of Superconducting Qubits*. PhD thesis, Yale University, 2013.
- [14] J. D. Strand, Matthew Ware, Félix Beaudoin, T. A. Ohki, B. R. Johnson, Alexandre Blais, and B. L. T. Plourde, *Phys. Rev. B* **87**, 220505 (2013).
- [15] Matthew Hutchings, J.B. Hertzberg, Y. Liu, N.T. Bronn, G.A. Keefe, J.M. Chow, and B. L. T. Plourde. *arXiv:1702.02253v1*.
- [16] Ioan Pop, Kurtis Geerlings, Gianluigi Catelani, Robert J. Schoelkopf, Leonid I. Glazman, and Michel H. Devoret, *Nature* **508**, 369 (2014).
- [17] Michel Devoret. in *Quantum Fluctuations (Les Houches Session LXIII)*, edited by S. Reynaud, E. Giacobino, and J. Zinn-Justin. Elsevier, 1997.
- [18] Fluxonium qubit built at Rigetti Computing.
- [19] R.H. Koch, D.P. Divincenzo, and Clarke J. *Phys. Rev. Lett.* **98**, 267003 (2007).
- [20] L. Faoro and L.B. Ioffe. *Phys. Rev. Lett.* **100**, 227005 (2008).
- [21] A.B. Zorin, F.-J. Ahlers, J. Niemeyer, T. Weimann, and H. Wolf, *Phys. Rev. B* **53**, 13682 (2014).
- [22] F.C. Wellstood, C. Urbina, and J. Clarke, *Appl. Phys. Lett.* **50**, 772 (1987).
- [23] D. J. Van Harlingen, T. L. Robertson, B. L. T. Plourde, P. A. Reichardt, T. A. Crane, and John Clarke, *Phys. Rev. B* **70**, 064517 (2004).
- [24] F. Yoshihara, K. Harrabi, A. O. Niskanen, Y. Nakamura, and J. S. Tsai, *Phys. Rev. Lett.* **97**, 167001 (2006).
- [25] P. J. J. O'Malley, J. Kelly, R. Barends, B. Campbell, Y. Chen, Z. Chen, B. Chiaro, A. Dunsworth, A. G. Fowler, I.-C. Hoi, E. Jeffrey, A. Megrant, J. Mutus, C. Neill, C. Quintana, P. Roushan, D. Sank, A. Vainsencher, J. Wenner, T. C. White, A. N. Korotkov, A. N. Cleland, and John M. Martinis, *Phys. Rev. Applied* **3**, 044009 (2015).
- [26] G. Ithier, E. Collin, P. Joyez, P. J. Meeson, D. Vion, D. Esteve, F. Chiarello, A. Shnirman, Y. Makhlin, J. Schrieffer, and G. Schön, *Phys. Rev. B* **72**, 134519 (2005).
- [27] P. Kumar, S. Sendelbach, M. A. Beck, J. W. Freeland, Zhe Wang, Hui Wang, Clare C. Yu, R. Q. Wu, D. P. Pappas, and R. McDermott, *Phys. Rev. Applied* **6**, 041001 (2016).